MUMT 618: Week #10

1 Conical Air Column Acoustics

In this section we analyze the acoustic properties of conic sections, or frusta.

1.1 Conical Bores: Modes of Propagation

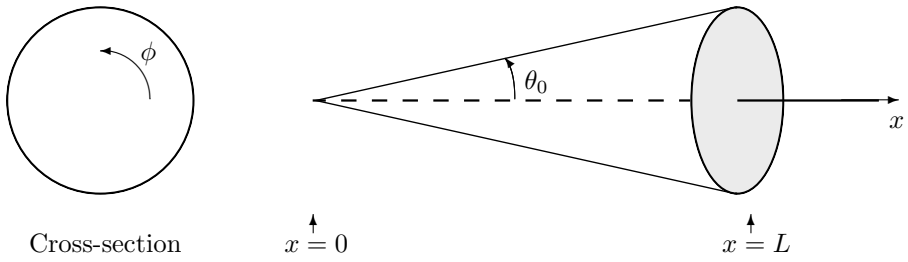

Figure 1: A conical section in spherical coordinates.

- A conical bore section in spherical coordinates (x, ϕ, θ) is depicted in Fig. 1. The wave equation in this geometric coordinate system is

$$\frac{1}{x^2}\frac{\partial}{\partial x}\left(x^2\frac{\partial p}{\partial x}\right) + \frac{1}{x^2\sin\theta}\frac{\partial}{\partial\theta}\left(\sin\theta\frac{\partial p}{\partial\theta}\right) + \frac{1}{x^2\sin^2\theta}\frac{\partial^2 p}{\partial\phi^2} = \frac{1}{c^2}\frac{\partial^2 p}{\partial t^2}. \tag{1}$$

- Longitudinal wave motion in conical bores is possible along orthogonal trajectories to the principal axis.

- While these transverse modes are only weakly excited in most musical instruments, they can become significant, for example, in the vicinity of a strongly flaring bell.

- Assuming sinusoidal solutions, this equation is separable in spherical coordinates, and the resulting differential equations describe sinusoidal wave motion, or standing-wave distributions, along each of the spherical coordinate axes.

- A complete general solution of the Helmholtz equation in spherical coordinates is then given by

$$P_{mn}(x, \phi, \theta) = \Phi(\phi)\Theta(\theta)X(x) = \frac{P_0}{(kx)^{\frac{1}{2}}}\cos(m\phi)\Theta_n^m(\cos\theta)J_{n+\frac{1}{2}}(kx), \tag{2}$$

  where $J_{n+\frac{1}{2}}(kx)$ is a Bessel function and $\Theta_n^m(y)$ are *associated Legendre functions.*

- The boundary condition at the cone wall, or at $\theta = \theta_0$, is $\partial p/\partial\theta = 0$, which can be met by adjusting the values of m and n so that an extremum of $\Theta_n^m(\cos\theta)$ occurs at the wall.

- Calculation of the Legendre functions for nonintegral n is nontrivial, and an accurate determination of cutoff frequencies for these modes is beyond the scope of this course. For axial symmetric waves ($m = 0$), Hoersch [1925] has presented a method for determining values of n that satisfy the boundary condition in conical horns of various angles.

- Typical values of θ_0 for saxophones, oboes, and bassoons are 2°, 1.5°, and 0.5°, respectively [Nederveen, 1969]. Using this procedure, the lowest values of n calculated for these angles are 109.27, 145.86, and 438.58, respectively.

- Computer calculations of the associated Legendre functions for integer values of n support these values and further indicate that solutions with $m = 1$ and n approximately equal to 53, 70, and 213, respectively are possible. These are nodal plane modes that correspond to the $(1, 0)$ mode in cylinders. Cutoff frequencies for these values of n are determined where the expression $k^2 - \beta^2/x^2$ becomes positive.

- The cutoff frequencies in a cone are dependent on x, so that waves of sinusoidal type having $\beta \neq 0$ are only possible in the outer or wider portions of a cone [Benade and Jansson, 1974]. Near the cone tip, any higher order modes that are excited will be evanescent.

- For the $m = 1$ mode solutions given above, the corresponding cutoff frequencies are approximately $f_c = 2.94/x$ kHz for saxophones, $f_c = 3.87/x$ kHz for oboes, and $f_c = 11.72/x$ kHz for bassoons, where x is given in meters.

- Alto saxophones, oboes, and bassoons have approximate lengths of 1 meter, 0.64 meters, and 2.5 meters, and thus transverse modes can propagate well within the audio spectrum at certain locations in these instruments.

- In comparison to cylindrical tubes, these higher modes propagate at much lower frequencies. However, excitation of the $m = 1$ mode requires transverse circular motion, which will not occur with any regularity in musical instruments. As mentioned with regard to cylindrical bores, evanescent mode losses may occur in a woodwind instrument mouthpiece and near toneholes.

1.2 Conical Bores: 1D Spherical Wave Propagation

- For musical purposes, the principal mode of wave propagation in conical tubes is spherical and along the central axis of the tube.

- Spherical waves of sound can theoretically propagate without reflection or loss away from the apex and along the principal axis of an infinite conical bore, assuming the walls are rigid, perfectly smooth, and thermally insulating.

- One-dimensional spherical-wave propagation along the central axis of the cone is possible for $m = 0$ and $\beta = 0$, in which case Eq. (2) reduces to a general solution of the form

$$P(x) = \frac{C^+}{x} e^{-jkx}, \tag{3}$$

  where C^+ is a constant and k is the wave number in open air. Waves of this type will propagate at all frequencies.

- During a steady-state excitation, sinusoidal pressure at position x in a finite length conic section is composed of superposed spherical traveling-wave components of the form

$$P(x,t) = \left[\frac{C^+}{x} e^{-jkx} + \frac{C^-}{x} e^{jkx} \right] e^{j\omega t}, \tag{4}$$

  where C^+ and C^- are complex amplitudes and sinusoidal time dependence is assumed.

- The associated volume velocity in the cone is found by rewriting Newton's second law for one-dimensional spherical waves as

$$\frac{\partial p}{\partial x} = -\frac{\rho}{A(x)}\frac{\partial U}{\partial t}, \tag{5}$$

where $A(x)$ is the surface area of a spherical cap that intersects the principal axis of the pipe at position x.

- For pressure waves of the form of Eq. (4), the corresponding volume flow is found using Eq. (5) as

$$\begin{aligned} U(x,t) &= \frac{A(x)}{x\rho c}\left[C^+\left(1+\frac{1}{jkx}\right)e^{-jkx} - C^-\left(1-\frac{1}{jkx}\right)e^{jkx}\right]e^{j\omega t}, \\ &= \frac{1}{x}\left[\frac{C^+}{Z_c(x)}e^{-jkx} - \frac{C^-}{Z_c^*(x)}e^{jkx}\right]e^{j\omega t}. \end{aligned} \tag{6}$$

- The wave impedance for spherical traveling-wave components propagating away from the cone apex is

$$Z_c(x) = \frac{P(x)}{U(x)} = \frac{\rho c}{A(x)}\left(\frac{jkx}{1+jkx}\right) = \frac{\rho c}{A(x)}\left(\frac{1}{1+\frac{1}{jkx}}\right), \tag{7}$$

which depends both on position x and frequency ω.

- The characteristic impedance for spherical traveling-wave components propagating in a cone toward its apex is given by $Z_c^*(x)$, or the complex conjugate of $Z_c(x)$.

- For $kx \gg 1$, the spherical wave fronts become more planar in shape and $Z_c(x)$ approaches $\rho c/A(x)$, the wave impedance for plane waves in a duct of cross section A.

- Near the apex of the cone, however, the imaginary part of $Z_c(x)$ becomes increasingly dominant and in the limit as $x \to 0$, the pressure and velocity traveling-wave components become 90° out of phase at the cone tip.

- It is intuitively helpful to rewrite the characteristic impedance in the form

$$Z_c(x) = \frac{1}{\frac{A(x)}{\rho c} + \frac{A(x)}{j\omega\rho x}}, \tag{8}$$

which is equivalent to the resistive wave impedance of a cylindrical bore in parallel with a lumped inertance of *acoustic* mass $\rho x/A(x)$.

- At low frequencies and near the conical apex, the inertance effectively shunts out the resistive element.

1.3 Finite Length Cones

- At any particular position x and frequency ω, sinusoidal pressure and volume velocity traveling-wave components are related by

$$P^+(x,\omega) = Z_c(x,\omega)\,U^+(x,\omega) \qquad P^-(x,\omega) = -Z_c^*(x,\omega)\,U^-(x,\omega) \tag{9}$$

with

$$P(x,\omega) = P^+(x,\omega) + P^-(x,\omega) \qquad U(x,\omega) = U^+(x,\omega) + U^-(x,\omega) \tag{10}$$

- The plus (+) superscripts indicate wave components traveling in the positive x-direction or away from the cone apex, while negative (−) superscripts indicate travel in the negative x-direction or toward the apex.

- These relationships are similar to those for the cylindrical bore, with the important difference that the characteristic impedance for waves traveling toward the cone tip is the complex conjugate of that for waves traveling away from the apex.

- In other words, wave propagation toward the apex is different from propagation away from the apex because a conical waveguide is nonsymmetric about its midpoint [Keefe, 1981, p. 70].
- Because the wave impedance for spherical-wave components is frequency dependent, these relationships are valid only for frequency-domain analyses.

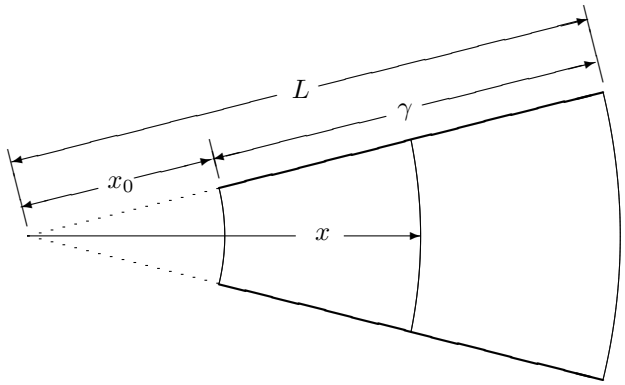

Figure 2: A divergent conical section and its associated dimensional parameters.

- Figure 2 illustrates a divergent conical frusta for which the apical section is truncated at $x = x_0$. The frequency-domain pressure wave reflectance and transmittance for such a section, assuming a load impedance Z_L at $x = L$, are given by

$$\frac{C^-}{C^+} = e^{-2jkL}\left[\frac{Z_L Z_c^*(L) - Z_c(L)Z_c^*(L)}{Z_L Z_c(L) + Z_c(L)Z_c^*(L)}\right], \tag{11}$$

and

$$\frac{p(L,t)}{C^+} = \frac{e^{-jkL}}{L}\left[\frac{Z_L Z_c(L) + Z_L Z_c^*(L)}{Z_L Z_c(L) + Z_c(L)Z_c^*(L)}\right], \tag{12}$$

respectively.

- The phase shift term e^{-2jkL} in Eq. (11) represents wave propagation to $x = L$ and back and has unity magnitude. The length parameter in this term is $2L$ because the cone apex is defined at $x = 0$.
- The $1/L$ factor in the transmittance is characteristic of conical waveguides and results from the spreading of pressure across an increasing surface area as the traveling-wave component of pressure propagates away from the cone apex [Benade, 1988].
- Equation 11 applies equally well to a convergent conical section and can be used to deduce the pressure reflectance at a conical apex by setting $Z_L = \infty$ and taking the limit as $x \to 0$. In this case, the term in brackets reduces to negative one.
- Thus, while the apex of a cone is a pressure antinode, pressure traveling-wave components reflect from the apex with an inversion, a behavior that at first appears paradoxical.
- It should be remembered that the boundary condition at the tip must be met by the sum of the two traveling-wave components and their corresponding $1/x$ factors. The inversion of reflected pressure is necessary to maintain a finite pressure at $x = 0$, which can then be determined by l'Hôpital's rule [Ayers et al., 1985].
- This behavior can also be explained in terms of pressure wave reflection at a rigid termination. Pressure wave components reflect from a rigid conical bore boundary with unity magnitude and a phase shift equal to $2 \angle Z_c$. Since the angle of $Z_c(0)$ is 90°, pressure is reflected from the tip with a 180° phase shift or with an inversion.

1.4 Input Admittance of a Conical Section

- The *input admittance* $Y(x)$ of a conical bore is more simply stated than its input impedance. For a conic section truncated at $x = x_0$, the input admittance is

$$Y_{in}(x_0) = \frac{1}{Z(x_0)} = \frac{U(x_0,t)}{P(x_0,t)} = \frac{A(x_0)}{\rho c}\left\{\left[\frac{e^{-jkx_0} - \frac{C^-}{C^+}e^{jkx_0}}{e^{-jkx_0} + \frac{C^-}{C^+}e^{jkx_0}}\right] + \frac{1}{jkx_0}\right\}, \tag{13}$$

  where the pressure wave reflectance C^-/C^+ is determined by the length of the bore and the boundary conditions at the opposite end, as discussed above.

- Equation (13) applies equally well to bores of increasing and decreasing diameter by using either positive or negative values of x.

- Equation (13) may be interpreted as a parallel combination of an acoustic inertance and a term reminiscent of the impedance of a cylindrical waveguide [Benade, 1988].

- The impedance of the acoustic inertance, which has an equivalent acoustic mass $\rho x_0/A(x_0)$, approaches infinity as $x_0 \to 0$.

- The input admittance seen from the open end (at $x = -L$) of a complete cone reduces to

$$\begin{aligned} Y_{in}(-L) &= \frac{A(L)}{\rho c}\left\{\left[\frac{e^{jkL} - \frac{C^-}{C^+}e^{-jkL}}{e^{jkL} + \frac{C^-}{C^+}e^{-jkL}}\right] - \frac{1}{jkL}\right\} \\ &= \frac{A(L)}{\rho c}\left\{\left[\frac{e^{jkL} + e^{-jkL}}{e^{jkL} - e^{-jkL}}\right] - \frac{1}{jkL}\right\} \\ &= \frac{A(L)}{j\rho c}\left[\cot(kL) - \frac{1}{kL}\right], \end{aligned} \tag{14}$$

  where the pressure reflectance at the cone apex ($x = 0$) is negative one.

- An open end at $x = -L$ can be approximated by the low-frequency estimate $Y_{in} = \infty$.

- The resonance frequencies of a complete cone ideally open at its large end are thus found at the infinities of Eq. (14), which are given for $n = 1, 2, \ldots$ by

$$f = \frac{nc}{2L}. \tag{15}$$

- The complete cone with open mouth has a fundamental wavelength equal to two times its length and higher resonances that occur at all integer multiples of the fundamental frequency, as was observed for open-open cylindrical pipes.

- The anti-resonances of the complete cone, however, do not fall exactly midway between its resonances, but are influenced by the inertance term in Eq. (14).

1.5 Truncated Cones

- Conical bores are always truncated to some extent to allow excitation at their small end. Assuming the mouth of the cone at $x = L$ is ideally open, so that $Z_L = 0$, the reflectance C^-/C^+ becomes $-e^{-2jkL}$ and the input admittance of a truncated cone reduces to

$$Y_{in}(x_0) = \frac{A(x_0)}{j\rho c}\left[\cot(k\gamma) + \frac{1}{kx_0}\right], \tag{16}$$

  where $\gamma = L - x_0$.

- If the small end of the cone, at $x = x_0$, is assumed ideally open, the resonance frequencies of the open-open (o-o) conic frustum are at the infinities of Eq. (16), which are given for $n = 1, 2, \ldots$ by

$$f^{(\text{o-o})} = \frac{nc}{2(L - x_0)} = \frac{nc}{2\gamma}. \tag{17}$$

- Thus, the higher natural frequencies of the open-open conic frustum are also related to the fundamental by integer multiple ratios.

- If the input end of the cone at $x = x_0$ is assumed ideally closed, which is nearly the case for reed-driven conical woodwind instruments, the resonance frequencies are found at the zeros of the input admittance.

- In this case, the partials of the closed-open conic frustum do not occur at exact integer multiples of the fundamental frequency, but are generally more widely spread apart depending on the magnitude of x_0.

- The natural frequencies of the truncated cone closed at its small end are found by solving the transcendental equation

$$\tan(k\gamma) = -kx_0. \tag{18}$$

  Equation (18) can be rewritten in the form

$$\tan\left(\pi \frac{f}{f_0}\right) = -\frac{\beta}{1-\beta}\left(\pi \frac{f}{f_0}\right), \tag{19}$$

  where $\beta = x_0/L$ and $f_0 = c/(2\gamma)$ is the fundamental frequency for the open-open conic frustum of length γ [Ayers et al., 1985].

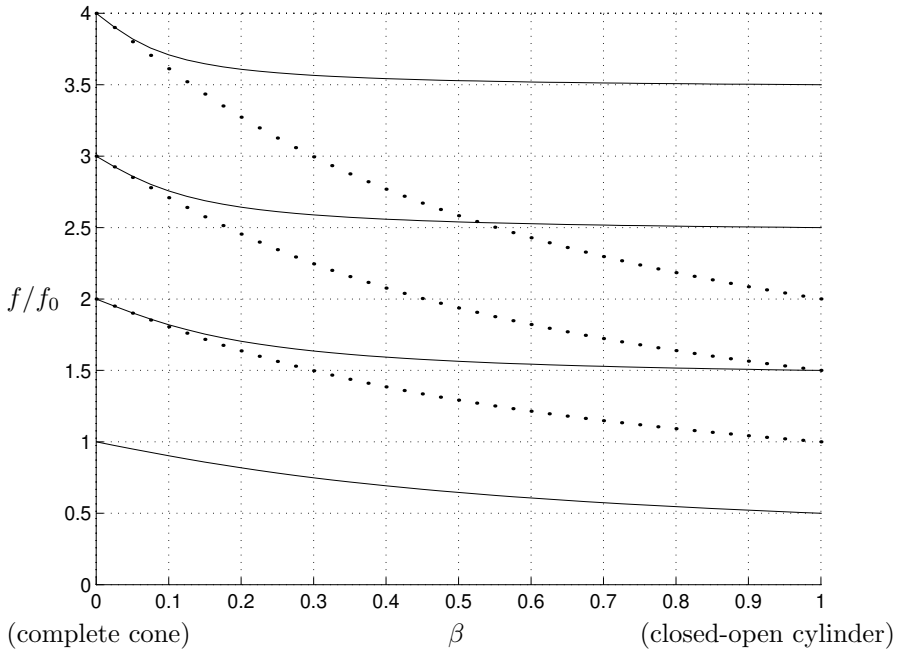

Figure 3: Partial frequency ratios, relative to f_0, for a closed-open conic frustum.

- Figure 3 illustrates the partial frequency ratios for a closed-open conic frustum, relative to the fundamental frequency of an open-open conic frustum of the same length, for $\beta = 0$ (complete cone) to $\beta = 1$ (closed-open cylinder).

- The dotted lines indicate exact integer relationships above the first partial and serve only to make more apparent the stretching of the partial ratios.
- The perfect harmonicity of the partials of an open-open conic frustum are distorted when a single-reed excitation mechanism is placed at one end.
- The fundamental frequency of the conic section is most affected by truncation and closure, as the inertance term in the admittance is largest for low frequencies.
- In terms of the fundamental wavelength of an open-open conic frustum of the same length, the inertance contributes a positive length correction that increases with truncation x_0 but decreases with frequency. Viewed in terms of the normal modes of a closed-open cylinder, however, the inertance contributes a negative length correction that is inversely proportional to truncation x_0 and frequency.

2 Conical Air Column Modeling

In this section, we look at the way wave propagation in conical air columns can be modeled using digital waveguide techniques.

2.1 Modeling a Single Conic Section

- Sound propagation in conical air columns can be well modeled by one-dimensional spherical waves traveling along the length of the cone.
- The one-dimensional wave equation for spherical pressure waves,

$$\frac{1}{x}\frac{\partial^2(xp)}{\partial x^2} = \frac{1}{c^2}\frac{\partial^2 p}{\partial t^2}\,, \tag{20}$$

  accurately represents lossless pressure wave propagation along the central axis of a conical tube, subject to the boundary conditions at both its ends.
- The continuous-time traveling-wave solution to this equation is

$$p(x,t) = \frac{f(t-x/c)}{x} + \frac{g(t+x/c)}{x}\,, \tag{21}$$

  where the functions $f(\cdot)$ and $g(\cdot)$ are completely general and continuous and can be interpreted as arbitrarily fixed waveshapes that travel in opposite directions along the x-axis with speed c.
- This expression is similar to that for plane waves with the exception that spherical pressure traveling-wave components are inversely proportional to their distance from the cone apex.
- A solution of this form can be discretized in time and space and given by [Smith, 1991]

$$p\left(t_n, x_m\right) = \frac{p^+(n-m)}{x} + \frac{p^-(n+m)}{x}. \tag{22}$$

- The behavior of a finite length conical bore can be approximated for low-frequency sound waves by assuming that pressure is equal to zero at an open end. This boundary condition is met with an inversion of traveling-wave pressure components at the open end.
- Figure 4 represents the digital waveguide implementation of ideal, lossless spherical-wave propagation in an ideally terminated conical tube.
- Aside from the $1/x$ scale factors, which are implemented at observation points, the cylindrical and conical waveguide implementations are exactly the same.
- Further, if the system input and output are measured at the same location, the $1/x$ scale factor is unnecessary.

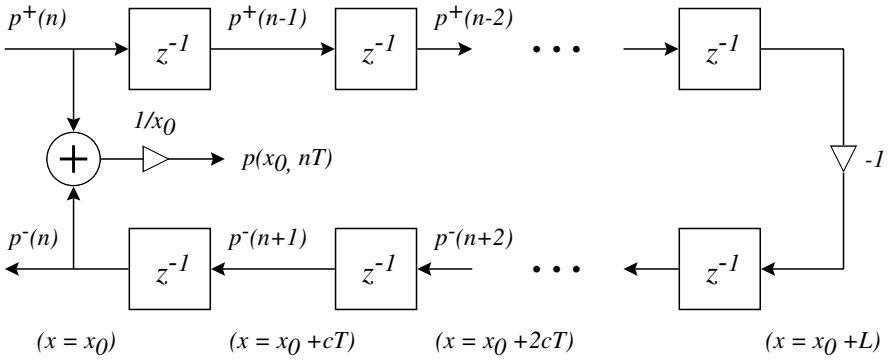

Figure 4: Digital waveguide implementation of ideal, lossless spherical-wave propagation in a conical tube.

2.2 Reflection at a Rigid Boundary

- In an earlier section, it was observed that pressure and volume flow traveling-wave components grow increasingly out of phase as they approach the cone apex. This behavior is defined by the complex characteristic impedance of conical air columns.
- The boundary condition imposed by a rigid termination requires that volume flow normal to the boundary equal zero.
- Where spherical volume velocity traveling-wave components reflect with an inversion, so that their sum is zero, spherical pressure traveling-wave components reflect with a phase angle $2\angle Z_c(x,\Omega)$.
- In the case of a complete cone, $\angle Z_c(0,\Omega) = 90°$, and pressure traveling-wave components reflect from the cone apex with a 180° phase shift (or an inversion).

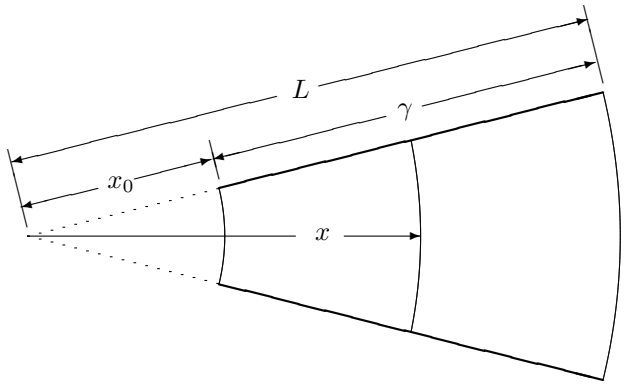

Figure 5: Divergent conical section rigidly terminated by a spherical cap at x_0.

- Figure 5 illustrates a divergent conical bore truncated and rigidly terminated at a distance x_0 from its apex.
- The pressure reflectance at x_0 is found from the boundary condition $U(x_0) = 0$, such that

$$\begin{aligned} U^+(x_0) + U^-(x_0) &= 0 \\ \frac{P^+(x_0)}{Z_c(x_0)} - \frac{P^-(x_0)}{Z_c^*(x_0)} &= 0 \end{aligned}$$

$$\Rightarrow \frac{P^+(x_0,s)}{P^-(x_0,s)} = \frac{Z_c(x_0,s)}{Z_c^*(x_0,s)} = \frac{jkx_0-1}{jkx_0+1}$$
$$= \left.\frac{x_0 s - c}{x_0 s + c}\right|_{s=jkc}, \tag{23}$$

where s is the Laplace transform variable and c is the speed of sound in air.

- As $x_0 \to 0$, the reflectance approaches negative one as observed above.
- Using the bilinear transform, this expression can be discretized as follows

$$\frac{P^+(x_0,z)}{P^-(x_0,z)} = \frac{-a_1 - z^{-1}}{1 + a_1 z^{-1}}, \tag{24}$$

where

$$a_1 = \frac{c - \alpha x_0}{c + \alpha x_0} \tag{25}$$

and α is the bilinear transform constant that controls frequency warping.

- Equation (24) is a first-order discrete-time allpass filter. This filter structure implements the $2\angle Z_c(x,\Omega)$ frequency-dependent phase delay experienced by pressure traveling-wave components reflecting from a rigid termination in a conical waveguide.
- The upper plot of Fig. 6 illustrates the continuous-time phase response of the reflectance given by Eq. (23) and the discrete-time phase response of the digital filter of Eq. (24).
- The lower plot of Fig. 6 indicates the allpass filter coefficient value as a function of cone truncation.
- As $x_0 \to 0$, the filter becomes unstable because $a_1 \to 1$ and the allpass pole falls on the unit circle. Thus, the truncation filter cannot be used to simulate a complete cone, but in this case the reflectance is simply negative one anyway.

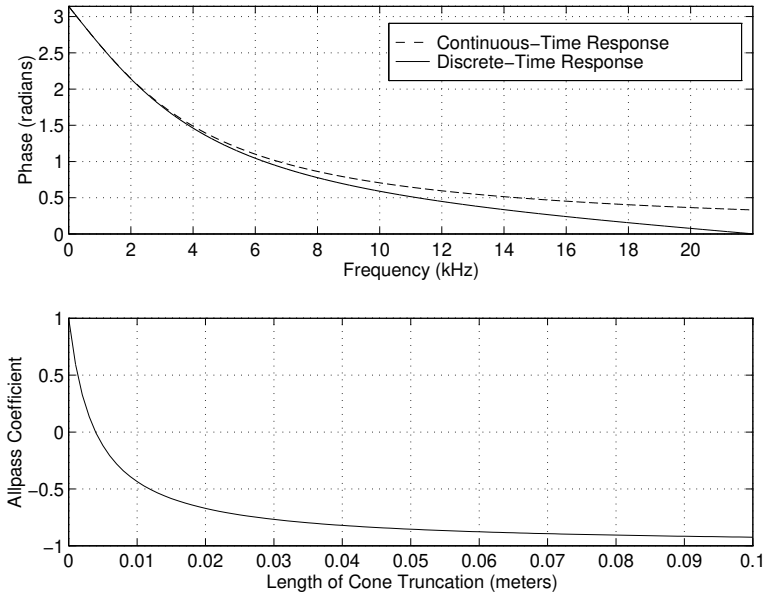

Figure 6: The conical truncation reflectance: (top) Continuous-time and discrete-time filter phase responses; (bottom) Digital allpass filter coefficient value versus x_0.

- The digital waveguide implementation of a closed-open conic section is shown in Fig. 7.
- The cone truncation reflectance filter is represented by $\mathcal{R}_{x_0}(z)$.

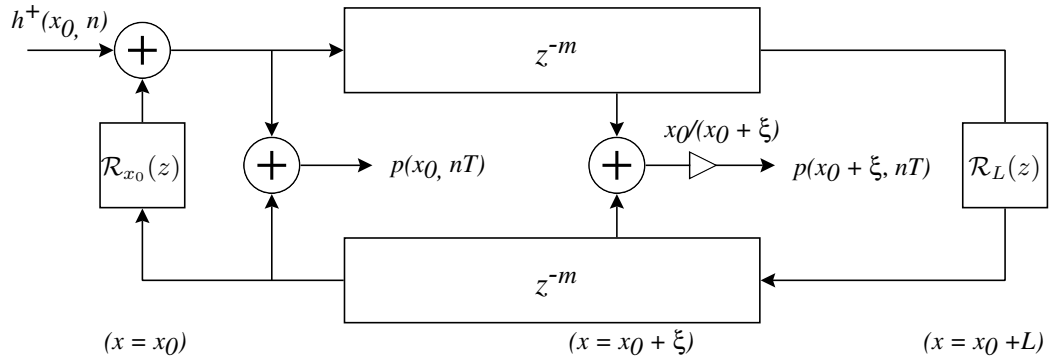

Figure 7: Digital waveguide implementation of a closed-open truncated conical section excited at $x = x_0$.

2.3 Input Impedance Calculations

- The waveguide "input impedance" $Z_{in}(x_0, \omega)$ for this system can be determined by calculating its response to a unit volume velocity impulse and transforming it to the frequency domain using the DFT.
- The continuous-time pressure response to a volume velocity impulse is given by the inverse Fourier transform of the characteristic impedance $Z_c(x, \Omega)$.
- This function is given by

$$h^+(x,t) = \frac{\rho c}{A(x)} \left[\delta(t) - \frac{c}{x}\, e^{-(c/x)t} \epsilon(t)\right], \tag{26}$$

  where $\epsilon(t)$ is the Heaviside unit step function.
- It is necessary to determine a digital filter that appropriately models the response of $h^+(x,t)$ in the discrete-time domain.
- The spherical-wave characteristic impedance is given in terms of its Laplace transform as

$$H_c^+(x,s) = Z_c(x,s) = \frac{\rho c}{A(x)} \left(\frac{xs}{c+xs}\right), \tag{27}$$

  where $A(x)$ is the spherical-wave surface area at x.
- Using the bilinear transform, an equivalent discrete-time filter is given by

$$H_d^+(x,z) = \left(\frac{\rho c}{A(x)}\right) \left(\frac{\alpha x}{c+\alpha x}\right) \frac{1-z^{-1}}{1+a_1 z^{-1}}, \tag{28}$$

  where α is the bilinear transform constant and a_1 is equal to the allpass truncation filter coefficient given in Eq. (25).
- The impulse response $h(x_0, n)$ of a closed-open truncated cone is found from the digital waveguide structure of Fig. 7 as the pressure response at $x = x_0$ to the impulse response $h^+(x_0, n)$.
- Because the cone is excited at $x = x_0$, output scale factors are appropriately weighted by x_0.
- Figure 8 is a plot of $h(x_0, n)$, calculated using a Levine and Schwinger model of the open-end radiation and neglecting viscothermal losses.
- Salmon [1946] and Benade [1988] proposed a transmission-line conical waveguide model directly analogous to that described above.

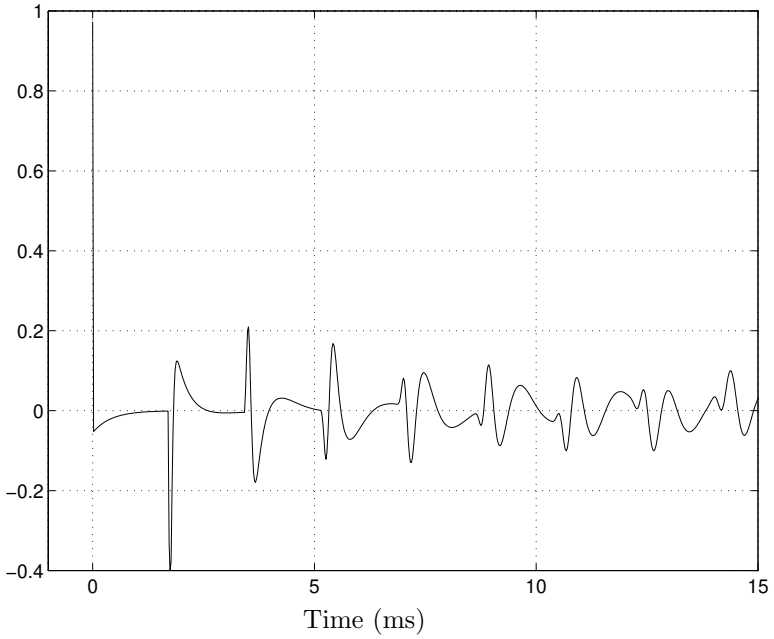

Figure 8: Impulse response of conical bore closed at $x = x_0$ and open at $x = L$. Open-end radiation is approximated by a 2nd-order discrete-time filter and viscothermal losses are ignored.

- Shown in Fig. 9, Benade's model represents a conic section by a cylindrical waveguide, a pair of "inertance" terms, and a transformer whose "turns ratio" is equal to the ratio P_{x_0}/P_L.
- The digital waveguide truncated cone model implements the cylindrical waveguide section using delay lines, as previously described, and the transformer operation wherever a physical pressure measurement is taken.

2.4 Diameter and Taper Discontinuities

A frequency-domain, transfer-matrix method for modeling piece-wise conical sections, as previously presented for cylindrical sections, is possible. The matrix elements are a bit more complicated, but the approach is well documented and validated and can include accurate characterizations of thermoviscous losses. In this section, however, we focus on the time-domain, traveling-wave approach for modeling combinations of conical sections.

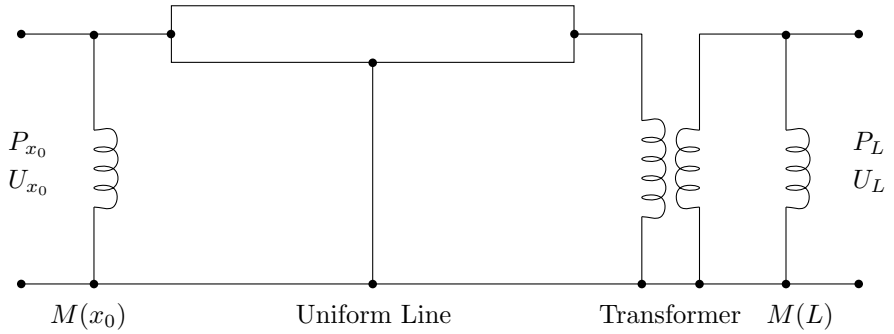

Figure 9: Equivalent circuit of a conical waveguide [after Benade [1988]].

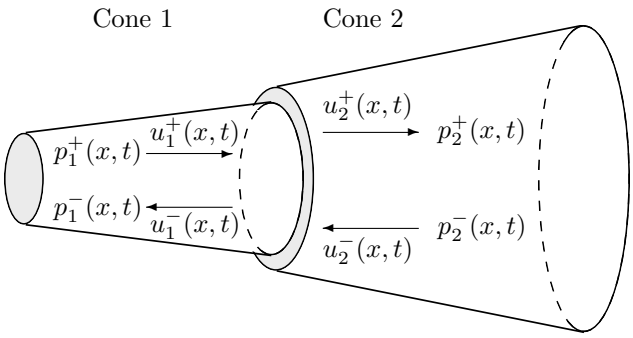

Figure 10: Junction of two conical tube sections.

- At the boundary of two discontinuous and lossless conical sections, Fig. 10, the abrupt change in diameter and rate of taper will cause scattering of traveling wave components.

- Assuming continuity of pressure and conservation of volume flow at the boundary,

$$P_1^+(\Omega) + P_1^-(\Omega) = P_2^+(\Omega) + P_2^-(\Omega) \tag{29}$$

and

$$P_1^+(\Omega)Y_{c1}(\Omega) - P_1^-(\Omega)Y_{c1}^*(\Omega) = P_2^+(\Omega)Y_{c2}(\Omega) - P_2^-(\Omega)Y_{c2}^*(\Omega), \tag{30}$$

where Y_{c1} is the characteristic admittance for section 1 at the boundary looking in the positive x direction.

- The characteristic admittance for spherical waves in a cone is given by

$$Y_c(x,\Omega) = \frac{1}{Z_c(x,\Omega)} = \frac{A(x)}{\rho c}\left(1 + \frac{1}{jkx}\right) \qquad Y_c^*(x,\Omega) = \frac{1}{Z_c^*(x,\Omega)} = \frac{A(x)}{\rho c}\left(1 - \frac{1}{jkx}\right), \tag{31}$$

where $Y_c(x,\Omega)$ applies to traveling-wave components propagating away from the cone apex in the positive x direction and $Y_c^*(x,\Omega)$ to traveling-wave components propagating toward the cone apex in the negative x direction.

- Solving for $P_1^-(\Omega)$ at the junction,

$$P_1^-(\Omega) = \left[\frac{Y_{c1}(\Omega) - Y_{c2}(\Omega)}{Y_{c1}^*(\Omega) + Y_{c2}(\Omega)}\right] P_1^+(\Omega) + \left[\frac{Y_{c2}(\Omega) + Y_{c2}^*(\Omega)}{Y_{c1}^*(\Omega) + Y_{c2}(\Omega)}\right] P_2^-(\Omega). \tag{32}$$

- The frequency-dependent scattering coefficient that relates $P_1^-(\Omega)$ to $P_1^+(\Omega)$ is

$$\begin{aligned} \mathcal{R}^-(\Omega) &= \frac{Y_{c1}(\Omega) - Y_{c2}(\Omega)}{Y_{c1}^*(\Omega) + Y_{c2}(\Omega)} \\ &= \frac{B-1}{B+1} - \frac{2B\gamma}{(B+1)(j\Omega + \gamma)}, \end{aligned} \tag{33}$$

where B is the ratio of wave front surface areas A_1/A_2 at the boundary and γ is given by

$$\gamma = -\frac{c}{A_1 + A_2}\left(\frac{A_1}{x_1} - \frac{A_2}{x_2}\right) \tag{34}$$

[Martínez and Agulló, 1988, Gilbert et al., 1990].

- This *reflectance* is given a negative superscript to indicate scattering in the negative x direction.

- The parameters x_1 and x_2 are measured from the (imaginary) apices of cones 1 and 2, respectively, to the discontinuity.

- Similarly, the expression for $P_2^+(\Omega)$ at the junction is

$$P_2^+(\Omega) = \left[\frac{Y_{c1}(\Omega) + Y_{c1}^*(\Omega)}{Y_{c2}(\Omega) + Y_{c1}^*(\Omega)}\right] P_1^+(\Omega) + \left[\frac{Y_{c2}^*(\Omega) - Y_{c1}^*(\Omega)}{Y_{c2}(\Omega) + Y_{c1}^*(\Omega)}\right] P_2^-(\Omega), \tag{35}$$

  and the reflectance that relates $P_2^+(\Omega)$ to $P_2^-(\Omega)$ is

$$\begin{aligned} \mathcal{R}^+(\Omega) &= \frac{Y_{c2}^*(\Omega) - Y_{c1}^*(\Omega)}{Y_{c2}(\Omega) + Y_{c1}^*(\Omega)} \\ &= \frac{1-B}{1+B} - \frac{2\gamma}{(1+B)(j\Omega+\gamma)}. \end{aligned} \tag{36}$$

- This reflectance is given a positive superscript to indicate scattering in the positive x direction.

- The scattering equations can then be expressed in terms of $\mathcal{R}^-(\Omega)$ and $\mathcal{R}^+(\Omega)$ as

$$P_1^-(\Omega) = \mathcal{R}^-(\Omega)P_1^+(\Omega) + \left[1 + \mathcal{R}^+(\Omega)\right] P_2^-(\Omega) \tag{37}$$

$$P_2^+(\Omega) = \left[1 + \mathcal{R}^-(\Omega)\right] P_1^+(\Omega) + \mathcal{R}^+(\Omega)P_2^-(\Omega). \tag{38}$$

- It is possible to define *transmittances* that indicate scattering through the junction as $\mathcal{T}^+(\Omega) = 1 + \mathcal{R}^-(\Omega)$ and $\mathcal{T}^-(\Omega) = 1 + \mathcal{R}^+(\Omega)$.

- These expressions are equally valid when either acoustic section is cylindrical, rather than conical. Replacing cone 1 by a cylindrical section, $x_1 = \infty$ and A_1 is given by the cylinder's cross-sectional area at the discontinuity.

- Whereas the junction scattering coefficients for cylindrical bore diameter discontinuities were real and constant, these expressions are frequency-dependent and must be transformed to discrete-time filters for time-domain implementation.

- Figure 11(a) illustrates the general scattering junction implementation for diameter and taper discontinuities in conical bores.

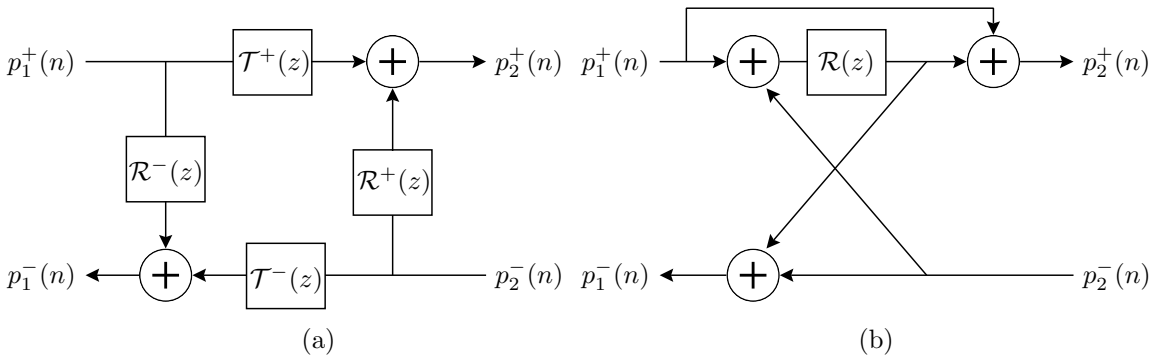

Figure 11: (a) The scattering junction for diameter and taper discontinuities in conical bores; (b) The one-multiply scattering junction for a taper discontinuity only [after [Välimäki, 1995]].

- Because $\mathcal{R}^-(\Omega)$ and $\mathcal{R}^+(\Omega)$ are different, the one-multiply form of the scattering junction implementation is not possible.

- However, if the wavefront surface areas are approximated by cross-sectional areas at the discontinuity, which is reasonable only for small changes in taper rate and cross-section, the reflectances $\mathcal{R}^-$ and $\mathcal{R}^+$ become identical for a discontinuity of taper only. In this case, a one-multiply scattering junction implementation is possible, as shown in Fig. 11(b) [Välimäki, 1995].
- Strictly speaking, however, the propagating wave fronts in cones are spherical and thus $\mathcal{R}^-$ and $\mathcal{R}^+$ will never be identical, even for a simple taper discontinuity.
- Equation (33) can be transformed to the time domain, resulting in the reflection function

$$r^-(t) = \frac{B-1}{B+1}\delta(t) - \frac{2B}{(B+1)}\gamma e^{-\gamma t}\epsilon(t), \tag{39}$$

  where $\delta(t)$ is the Dirac impulse and $\epsilon(t)$ is the Heaviside unit step function [Martínez and Agulló, 1988].
- An appropriate discrete-time filter is found by making the bilinear transform frequency variable substitution in Eq. (33) with the result

$$\mathcal{R}^-(z) = \frac{B-1}{B+1} - \frac{2B\gamma/(\alpha+\gamma)}{(B+1)}\left(\frac{1+z^{-1}}{1-a_1 z^{-1}}\right), \tag{40}$$

  where γ is as given in Eq. (34), α is the bilinear transform constant, and

$$a_1 = \frac{\alpha-\gamma}{\alpha+\gamma} \tag{41}$$

  is the first-order filter pole location in the $z-$plane.
- Unfortunately, $\mathcal{R}^-(z)$ is unstable for negative γ, which occurs any time cone 2 has a lower rate of taper than cone 1.
- Equivalently, $\mathcal{R}^-(\Omega)$ has no causal inverse Fourier transform for negative γ.
- This corresponds to a growing exponential in the reflection function $r^-(t)$.
- The reflectance is a junction characteristic that is "blind" to the boundary conditions upstream or downstream from it. Physically realistic boundary conditions in such cases, however, will always limit the time duration over which the growing exponential can exist.
- Experimental measurements of reflection functions due to discontinuities have verified this general behavior [Agulló et al., 1995].
- The problem here in terms of digital waveguide modeling, is that the growing exponentials become unstable digital filters in the discrete-time domain.

3 Synthesizing Conical Instrument Sounds

This section was adapted from the paper *Time-Domain Synthesis of Conical Bore Instrument Sounds* in *Proceedings of the 2002 International Computer Music Conference* by Gary P. Scavone [Scavone, 2002]. The goal of this study was to develop a simple and efficient model for synthesizing the sounds of instruments with conical air columns.

3.1 The "Reed" Model

- For this study, we will explore digital waveguide techniques for achieving realistic conical bore instrument sounds.
- A simple memory-less, non-linear reed function is used for the realtime implementations discussed here.

- The reed-channel volume flow and pressure difference characteristic, shown in Fig. 12, is solved in terms of a non-linear traveling-wave reflection function [Smith, 1986] as:

$$p_d^+ = r(p_\Delta)\left[p_d^- - \frac{p_u}{2}\right] + \frac{p_u}{2},$$

where

$$r(p_\Delta) = \frac{Z_r(p_\Delta) - Z_o}{Z_r(p_\Delta) + Z_o},$$

p_d is the pressure on the downstream side of the reed, p_u is the player's breath pressure (upstream), $p_\Delta = p_u - p_d$ is the pressure difference across the reed, Z_r is a time-varying reed "impedance", and Z_o is the real wave impedance at the air column input.

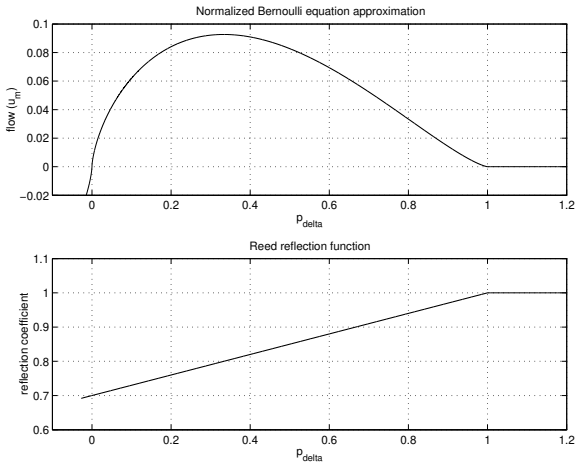

Figure 12: Bernoulli static flow expression (top); Simplified reed reflection function (bottom).

- Good results have been achieved using the simplified reed reflection function shown at the bottom of Fig. 12 in clarinet synthesis algorithms.
- While the behavior of the reed function plays an important role in the overall quality of a synthesis model, the memory-less system is adequate for the purposes of evaluating the various air column models explored here.

3.2 The Conical Waveguide

- Wave propagation along the principal axis of a conic frustum can be solved in terms of one-dimensional traveling *spherical* waves with *complex, location-dependent* wave impedance.
- In general, expressions describing the interaction of spherical waves will be frequency-dependent, while those for plane-wave scattering are often simple scalar functions.

3.3 The Equivalent Circuit

- The acoustic properties of a conic frustum can be represented by an equivalent circuit consisting of a uniform transmission line, two acoustic inertances, and a transformer, as shown in Fig. 14 [Benade, 1988].
- This representation suggests that a conical air column model can be implemented using a cylindrical waveguide, a scalar "turns ratio" multiplier, and appropriately designed inertance components at each end of the waveguide.

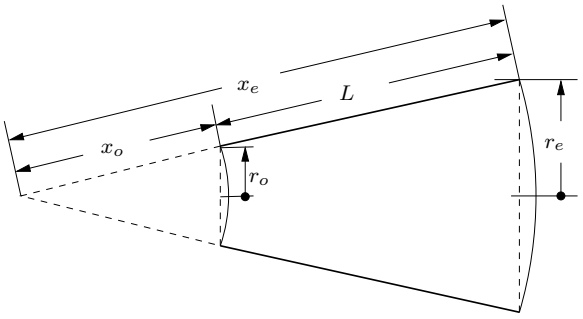

Figure 13: A conical waveguide.

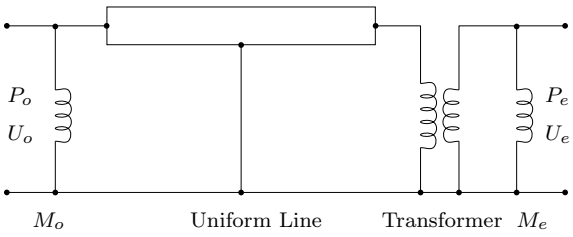

Figure 14: Equivalent circuit of a conical waveguide.

- An ideal open end, represented by a load impedance of zero, will "short-circuit" an input/output inertance.
- The equivalent circuit for an open-open conic frustum then reduces to a uniform transmission line and a scalar transformer term.
- This confirms the fact that a cylindrical pipe open at both ends and an open-open conic section, each of length L, have equivalent longitudinal mode frequencies given by $f_n = nc/2L$, $n = 1, 2, 3, \ldots$, where c is the speed of wave propagation within the structures.
- A pressure-controlled wind instrument excitation mechanism, such as a saxophone reed-mouthpiece or trumpet player lip-reed, functions as a nearly rigid, time-varying termination at an air column input.
- When attached to the input of a conical waveguide, the parallel driver impedance and input inertance (M_o) combination plays a significant role in determining the overall behavior of the air column.

3.4 Properties of Conic Frusta

- It is generally agreed that harmonically aligned air column mode ratios better support a stable "regime of oscillation" via mode cooperation [Worman, 1971].
- It is thus expected that a synthesis model incorporating a nonlinear excitation mechanism will likewise benefit from such mode cooperation in attempting to produce a robust, stable oscillatory regime.
- Ayers et al. [1985] presents an exploration of the properties of conic frusta. Of particular note, the mode ratios for truncated closed-open frusta of length L are shown to vary with respect to the parameter β as depicted in Fig. 15.
- β can be defined in terms of the ratio of input to output end radii, r_o/r_e, or in terms of the ratio $x_o/(x_o + L)$, where x_o is the length of the missing, truncated apical section (see Fig. 13).

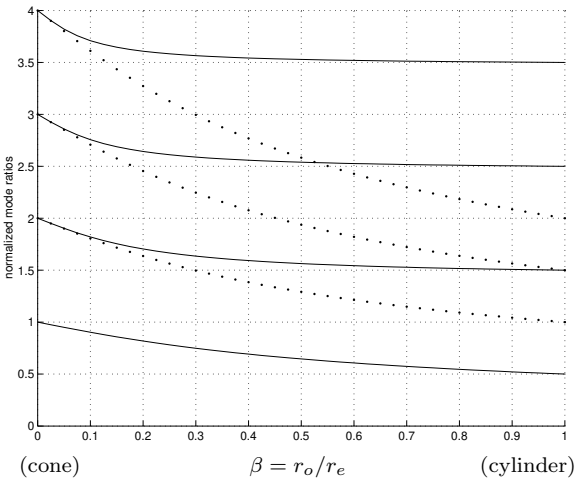

Figure 15: Mode frequencies for a closed-open conic frustum normalized by the fundamental frequency of an open pipe of the same length as the frustum. The dotted curves indicate integer relationships to the first mode.

- A complete cone is given by $\beta = 0$, while a closed-open cylinder is given by $\beta = 1$.
- It should be obvious from Fig. 15 that any closed-open truncated conical section will have inharmonic mode ratios and that the extent of this inharmonicity is dependent on the dimensions of the frustum.
- Attempts at robust synthesis using a model that correctly simulates the behavior of a truncated conical section may in turn be hindered.
- Benade [1976] reports that the effects of truncation can be reduced by utilizing a reed/mouthpiece cavity with an equivalent volume equal to that of the missing conical section.
- This constraint is based on a lumped characterization of the reed/mouthpiece cavity, which is only appropriate for low-frequency modes whose wavelengths are large in comparison to the dimensions of the cavity.
- Higher-frequency modes are less likely to benefit from such a change because they are more directly affected by changes in waveguide shape.
- Figure 16 plots the mode ratios for a cylinder-cone compound horn designed so that the cylindrical section volume is equal to the truncated conic section volume.
- For $\beta = 1$, the structure is of infinite length and all its modes converge to zero. In comparison with Fig. 15, the compound horn displays nearly harmonic mode ratios out to values of β in the range 0.2–0.3.
- Another property of conic frusta can be directly attributed to the input inertance element, M_o, in the equivalent circuit (Fig. 14). The inertance, whose magnitude varies with the parameter β, tends to "shunt" low-frequency wave components, thus imposing a "high-pass" characteristic on the resulting air column mode structure.
- For longer conic sections, the lowest modes can be significantly attenuated, which in turn destabilizes oscillatory regimes dependent on these modes. This behavior is often apparent in the lowest notes of saxophones, which tend to be difficult to control under soft playing conditions.
- Figure 17 shows an example conic section input impedance in which this effect is demonstrated. The smooth curve indicates the combined influence of the conicity inertance and the open-end load impedance.

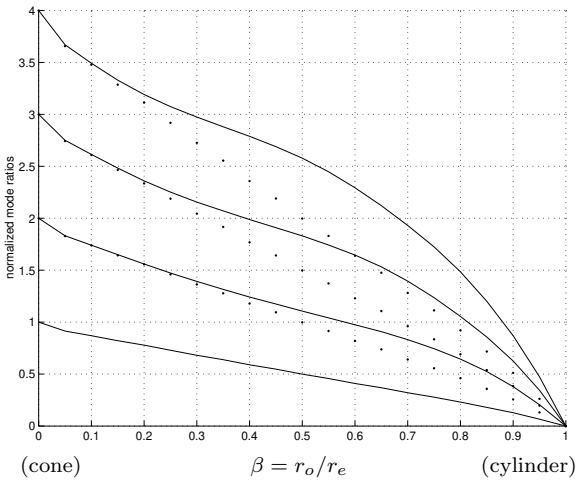

Figure 16: Mode frequencies for a closed-open, cylinder-cone compound horn in which the cylindrical section volume is equivalent to the missing conic section volume. The dotted curves indicate integer relationships to the first mode.

3.5 Modeling Approaches

- In order to implement the equivalent circuit of a conical waveguide using digital waveguide techniques, it is necessary to express the lumped impedance elements of Fig. 14 in terms of traveling-wave parameters and then convert these expressions to discrete-time filters.
- The impedance of the input inertance, given in terms of a Laplace transform, is $M_o(s) = (\rho x_o/A_o)\, s$, where ρ is the mass density of air, A_o is the area of the spherical wavefront at the waveguide input, and s is Laplace transform frequency variable.
- The effective impedance at the waveguide input is determined as the parallel combination of M_o and an input load impedance. If the input is rigidly terminated, the input load is infinite and the pressure-wave reflectance is given by:

$$\mathcal{R}_o(s) \triangleq \frac{P_o^-(s)}{P_o^+(s)} = \frac{M_o(s) - Z_o}{M_o(s) + Z_o} = \frac{x_o s - c}{x_o s + c},$$

  where $Z_o = \rho c/A_o$ is a real, locally defined characteristic impedance parameter.
- The reflectance filter, discretized with the bilinear transform, is

$$\mathcal{R}_o(z) = \frac{-a_1 - z^{-1}}{1 + a_1 z^{-1}}, \quad \text{where} \quad a_1 = \frac{c - \alpha x_o}{c + \alpha x_o},$$

  and α is the bilinear transform constant that controls frequency warping.
- This first-order allpass filter accurately accounts for the phase delay experienced by pressure traveling-wave components reflecting from a rigid input termination in a conical waveguide.
- The output inertance, M_e, tends to be less significant than that at the input, particularly in the presence of an open-end load impedance. In general, a single output reflectance filter can be designed based on the parallel combination of M_e and an appropriate open-end impedance characterization.
- Figure 18 shows a truncated conic structure and the corresponding digital waveguide block diagram, using input and output reflectance filters as discussed above.
- The goal here is to model a conical bore instrument system by attaching a simple, memory-less, nonlinear excitation mechanism to a conical air column representation.

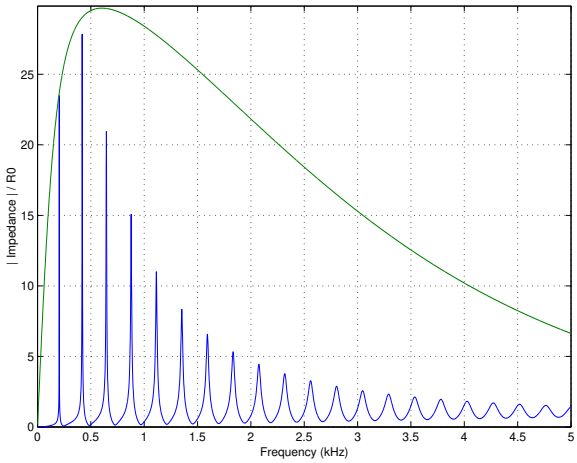

Figure 17: An example conic frustum input impedance.

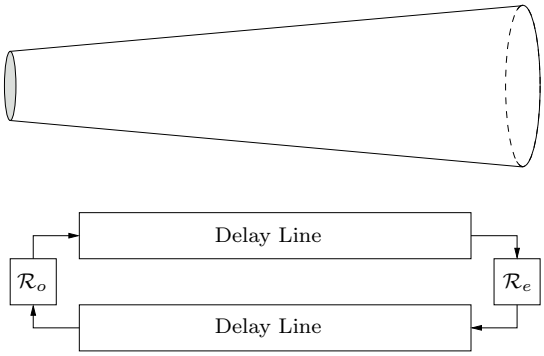

Figure 18: A closed-open conic structure (top) and its digital waveguide block diagram (bottom).

- The traditional reed function/air column coupling, however, is derived for an input cylindrical section using a real wave impedance. It is not a simple process to re-derive the reed function using the complex wave impedance of a conic frustum. Even if we ignored this complication, direct coupling of the reed function to the allpass inertance element at the input to the conical "circuit" would produce a delay-free loop in the digital waveguide implementation. These constraints lead to the modeling approach discussed first in this section.

3.6 The "Cyclone"

- The "cyclone" conical bore model is based on a compound cylindrical-conical segment air column model as illustrated at the top of Fig. 19.
- The input cylindrical section roughly models the instrument mouthpiece cavity and its use avoids the complications previously discussed with respect to the non-linear driver.
- In addition, the cylindrical section can be designed to have an equivalent volume equal to the missing conic section volume. Assuming no diameter discontinuity at the cylinder-cone junction, this constraint is met using a cylindrical section length equal to $x_o/3$.
- It should be noted that Benade distinguishes between a cavity's physical and equivalent volumes under

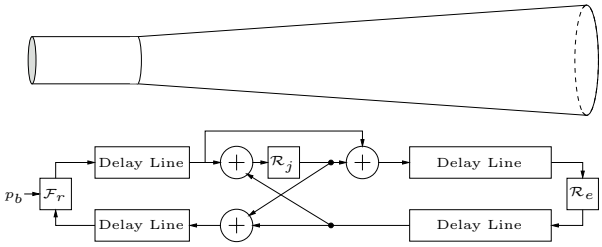

Figure 19: "Cyclone" physical structure (top) and digital waveguide block diagram (bottom).

playing conditions, which are typically not the same. For the simplified reed function used in this implementation, however, it is reasonable to ignore this difference.

- The cylinder-cone junction filter is derived assuming continuity of pressure and conservation of volume velocity and then discretized using the bilinear transform as:

$$\mathcal{R}_j^-(z) = \mathcal{R}_j^+(z) = -\frac{\gamma}{\alpha+\gamma}\left(\frac{1+z^{-1}}{1-a_1 z^{-1}}\right),$$

where α is the bilinear transform constant,

$$\gamma = \frac{c}{2x_o}, \qquad a_1 = \frac{\alpha-\gamma}{\alpha+\gamma},$$

c is the speed of wave propagation in the structure, and x_0 is the length of the truncated conic section.

- This expression could just as well have been derived from the parallel combination of the input inertance M_o and the wave impedance of the input cylindrical section.
- The junction transmittance magnitude response ($|1+\mathcal{R}|$) is shown in Fig. 20 for various values of x_o.

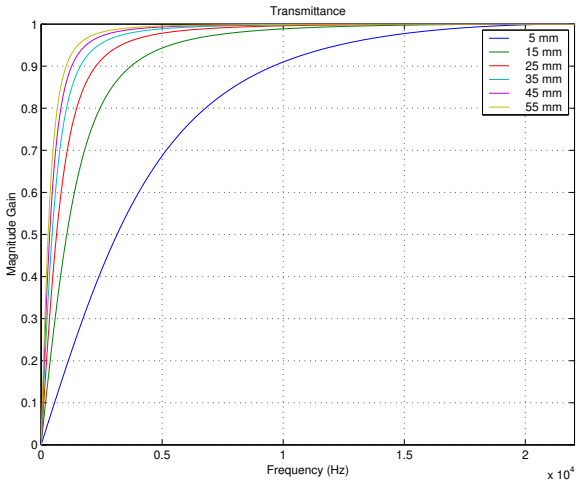

Figure 20: The cylinder-cone junction transmittance for various values of truncation x_o.

- The "high-pass" filter characteristic associated with the conical waveguide input inertance term can vary significantly depending on the frustum dimensions.

- Shorter values of x_o correspond to steeper flare rates, which produce greater wave discontinuity at the junction and greater low-frequency attenuation.
- While this might appear to imply a preference for less steeply flared conic sections, it should be remembered that larger values of x_0 correspond to larger values of β in Fig. 15 and thus greater mode inharmonicity. The result is a design conflict between junction discontinuity, which destabilizes the lower air column modes, and mode harmonicity.
- The cylinder-cone junction can be implemented using a single first-order digital filter, as discussed by Smith [1991], Välimäki and Karjalainen [1994] and others. A block diagram of the resulting digital waveguide model is shown in Fig. 19.
- Figure 21 displays the input impedance and sound spectrum produced by an example "cyclone" waveguide model.

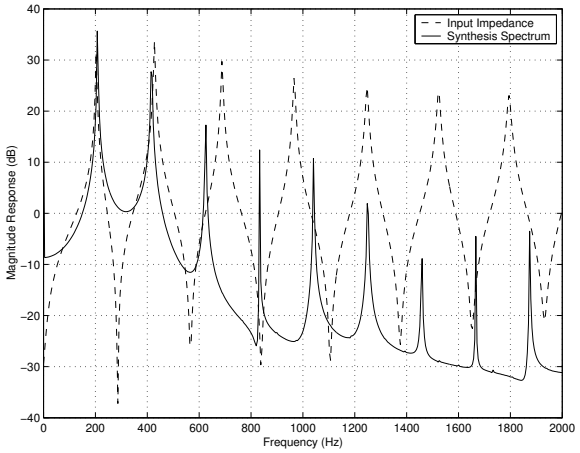

Figure 21: Example "cyclone" model input impedance and synthesized sound spectrum.

- Despite significant inharmonicity of the input impedance peaks, the resulting synthesis spectrum is harmonic and exhibits contributions from "misaligned" peaks as a result of the non-linear regenerative process.
- The sounds produced by the "cyclone" model have a distinctive saxophone quality, though the instabilities associated with truncated conic frusta as outlined in earlier sections are present and the functional parameter space can be difficult to assess.

3.7 The Cylindrical Saxophone

- With the help of Fig. 14, we can develop an alternative interpretation of the "cyclone" model as two uniform transmission-line elements separated by a shunt inertance component.
- If the inertance is implemented as a small, mass-like "register hole", we have the physical structure shown in Fig. 22 and a model that is equivalent to Benade's "cylindrical saxophone" [Benade, 1988].
- The impedance of an open-hole shunt inertance, given in terms of a Laplace transform, is:

$$Z(s) = \frac{\rho t}{A_h} s,$$

where t is the effective height of the hole and A_h is its cross-sectional area.

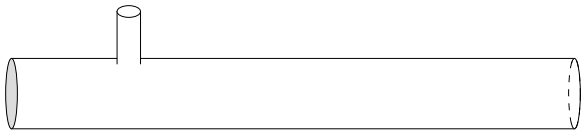

Figure 22: The "cylindrical saxophone" model.

- The junction filter derived for the register hole is [Scavone and Cook, 1998]

$$\mathcal{R}_j^-(z) = \mathcal{R}_j^+(z) = -\frac{\gamma}{\alpha+\gamma}\left(\frac{1+z^{-1}}{1-a_1 z^{-1}}\right),$$

  where α is the bilinear transform constant,

$$\gamma = \frac{cA_h}{2tA_o}, \qquad a_1 = \frac{\alpha-\gamma}{\alpha+\gamma},$$

  and A_o is the cross-sectional area of the cylindrical pipe.

- The "cyclone" and "cylindrical" circuits are equivalent with parameters related by:

$$x_o = \frac{A_o t}{A_h} \quad \text{or} \quad t = \frac{x_o A_h}{A_o}.$$

- It is interesting to compare the corresponding conic frustum and register hole parameters. We see that the length of the truncated conic section is proportional to register hole height and inversely proportional to register hole radius.

- The "cylindrical" model parametrization scheme has the added benefit of allowing synthesis of either a clarinet or a saxophone-like system via control of the filter gain parameter γ.

- The register hole is effectively closed when its radius is zero, which results in $\gamma = 0$ and $\mathcal{R}_j(z) = 0 \; \forall \; z$. Since there is no junction discontinuity, the system reduces to a single continuous cylindrical section.

- The "cylindrical saxophone" model presents a slightly more complex parameter space (parameters t and A_h versus x_o), though its response is similar to the "cyclone" model.

3.8 The Virtual "Blowed String"

- The "cyclone" and "cylindrical saxophone" models offer acoustically accurate representations of their corresponding physical manifestations.

- In addition, they inherit the various potential disadvantages previously discussed for these structures, including modal inharmonicity and weak low frequency mode support. An accurate physical model does not always make the best musical instrument.

- It is an interesting exercise to throw physical reality aside and to consider a more abstract approach to the design of an acoustic air column or resonator.

- In order to synthesize conical bore instrument sounds using a pressure-controlled driving mechanism, we desire a stable structure with the following features:

  - resonance frequencies given by $nc/2L$, for $n = 1, 2, 3, \ldots$
  - an input point with sufficient pressure fluctuation to drive a reed function.

- An open-open cylinder possesses the desired modal characteristic. However, air pressure variations are constrained to zero at an open pipe end, or pressure node.

- Another system possessing the desired resonance structure is a stretched string, fixed at both its ends. The string and open pipe share a variety of analogous properties via an exchange of mechanical and acoustic variables.
- Likewise, there are similarities in the way that each system can be driven. A string can be bowed, plucked, or struck at any point along its length except near either of its ends, where the mechanical velocity is constrained to zero.
- By analogy, it should be possible to drive an open pipe by applying a pressure-controlled excitation at any point along its length other than near an open end.
- This possibility has not been realized because no appropriate pressure-controlled device has been developed that can be positioned inside a pipe without modifying its acoustic properties.
- Digital synthesis systems, however, are not limited by the physical constraints of reality.
- Inspired by the bowed string, the "blowed string" model incorporates an open-open cylindrical air column structure and a non-linear reed function, applied at a "blowing" point that can be varied along the length of the pipe.
- The "blowed string" digital waveguide block diagram is shown in Fig. 23.

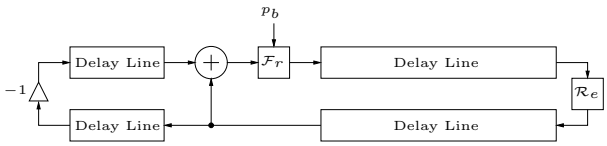

Figure 23: "Blowed string" block diagram.

- One end of the pipe is modeled with a lossy reflectance filter $\mathcal{R}_e$, while the other end is represented by an ideal impedance of zero (which corresponds to the pressure wave multiplier -1).
- The internal pressure at any point within the air column is calculated by summing the two traveling-wave components. The reed function uses the internal pressure value, together with the current "blowing" pressure, to determine an appropriate function output.
- The actual "blowed string" implementation can be simplified with respect to the block diagram of Fig. 23. In practice, each delay-line pair can be combined into a single unit and the scalar multiplier can be commuted to a more convenient implementation point.
- Thus, the entire system can be implemented using two interpolating delay lines, a simple first-order lowpass filter, an adder, and a non-linear reed reflection function. It is even possible to use just a single delay line with a fractional-delay tap output.
- Variation of the blow point can provide a wide range of timbres. The relationship between bow position and harmonic content of a bowed-string sound applies to this structure as well.
- When "blowed" at $1/n$th the distance from a pipe end, modes at integer multiples of n are not excited.
- By positioning the "blow point" at the center of the air column, the characteristic timbre of a clarinet is achieved. In addition to being the most computationally efficient model discussed, the "blowed string" displays exceptionally robust behavior over a wide parameter space.
- Figure 24 displays the input impedance and sound spectrum produced by the "blowed string" waveguide model with a "blow" point positioned at 1/5 the distance from an open end.
- The attenuation of the 5th harmonic is clearly evident. In general, there is significantly more harmonic content in this sound than was present in the previously discussed models.

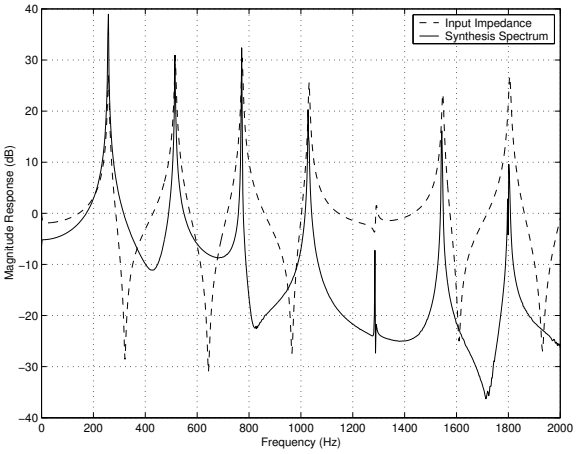

Figure 24: Example "blowed string" model input impedance and synthesized sound spectrum.

3.9 Summary

- The "cyclone" and "cylindrical saxophone" approaches to conical bore modeling provide acoustically accurate representations of their respective physical systems. For the purposes of acoustic study and further explorations regarding the properties of conic frusta, these models offer efficient structures for discrete-time implementation. In addition, the two equivalent parameterization schemes provide an interesting duality and perspective on the acoustic behavior of conical waveguides. With respect to synthesis, these models produce good sonic results within a somewhat complex parameter space.
- The virtual "blowed string", though potentially less appealing to acoustic purists, provides a robust and flexible synthesis model capable of generating a wide range of possible timbres, including both cylindrical and conical bore sounds. This model suggests an interesting analogy to the bowed string based on an abstract or "physically informed" view of air column acoustics.

References

J. Agulló, S. Cardona, and D. Keefe. Time-domain deconvolution to measure reflection functions for discontinuities in waveguides. *Journal of the Acoustical Society of America*, 97(3):1950–1957, Mar. 1995.

D. R. Ayers, L. J. Eliason, and D. Mahgerefteh. The conical bore in musical acoustics. *American Journal of Physics*, 53(6):528–537, June 1985.

A. H. Benade. *Fundamentals of Musical Acoustics*. Oxford University Press, New York, 1976.

A. H. Benade. Equivalent circuits for conical waveguides. *Journal of the Acoustical Society of America*, 83 (5):1764–1769, May 1988.

A. H. Benade and E. Jansson. On plane and spherical waves in horns with nonuniform flare: I. Theory of radiation, resonance frequencies, and mode conversion. *Acustica*, 31(2):80–98, Feb. 1974.

J. Gilbert, J. Kergomard, and J. D. Polack. On the reflection functions associated with discontinuities in conical bores. *Journal of the Acoustical Society of America*, 87(4):1773–1780, Apr. 1990.

V. A. Hoersch. Non-radial harmonic vibrations within a conical horn. *Physics Review*, 25:218–224, 1925.

D. H. Keefe. *Woodwind Tone-hole Acoustics and the Spectrum Transformation Function*. PhD thesis, Case Western Reserve University, 1981.

H. Levine and J. Schwinger. On the radiation of sound from an unflanged circular pipe. *Physics Review*, 73 (4):383–406, Feb. 1948.

J. Martínez and J. Agulló. Conical bores. Part I: Reflection functions associated with discontinuities. *Journal of the Acoustical Society of America*, 84(5):1613–1619, Nov. 1988.

C. J. Nederveen. *Acoustical Aspects of Woodwind Instruments*. Frits Knuf, Amsterdam, The Netherlands, 1969.

V. Salmon. Generalized plane wave theory of horns. *Journal of the Acoustical Society of America*, 17: 199–211, 1946.

G. P. Scavone. Time-domain synthesis of conical bore instrument sounds. In *Proceedings of the 2002 International Computer Music Conference*, pages 9–15, 2002.

G. P. Scavone and P. R. Cook. Real-time computer modeling of woodwind instruments. In *Proceedings of the International Symposium on Musical Acoustics, Leavenworth, WA*, pages 197–202, June 1998.

J. O. Smith. Efficient simulation of the reed-bore and bow-string mechanisms. In *Proceedings of the 1986 International Computer Music Conference*, pages 275–280, The Hague, Netherlands, 1986. Computer Music Association.

J. O. Smith. Waveguide simulation of non-cylindrical acoustic tubes. In *Proceedings of the 1991 International Computer Music Conference*, pages 304–307, Montreal, Canada, 1991. Computer Music Association.

V. Välimäki. *Discrete-Time Modeling of Acoustic Tubes Using Fractional Delay Filters*. PhD thesis, Helsinki University of Technology, Faculty of Electrical Engineering, Laboratory of Acoustic and Audio Signal Processing, Espoo, Finland, Report no. 37, Dec. 1995.

V. Välimäki and M. Karjalainen. Digital waveguide modeling of wind instrument bores constructed of truncated cones. In *Proceedings of the 1994 International Computer Music Conference*, pages 423–430, Århus, Denmark, 1994. Computer Music Association.

W. E. Worman. *Self-Sustained Nonlinear Oscillations of Medium Amplitude in Clarinet-Like Systems*. PhD thesis, Case Western Reserve University, 1971.